SIAM J. SCI. COMPUT.
Vol. 42, No. 3, pp. B792–B815





# APPROXIMATION TO SINGULAR QUADRATIC COLLISION MODEL IN FOKKER–PLANCK–LANDAU EQUATION*

RUO LI†, YANLI WANG‡, AND YIXUAN WANG§

**Abstract.** We propose a Hermite–Galerkin spectral method to numerically solve the spatially homogeneous Fokker–Planck–Landau equation with a singular quadratic collision model. To overcome the difficulty of the computationally expensive collision model, we adopt a novel approximation formulated by a combination of a simple linear term and a quadratic term very expensive to evaluate. Using the Hermite expansion, the quadratic term is evaluated exactly by calculating the spectral coefficients. To deal with singularities, we make use of Burnett polynomials so that even a very singular collision model can be handled smoothly. Numerical examples demonstrate that our method can capture low-order moments with satisfactory accuracy and performance.

**Key words.** Fokker–Planck–Landau equation, Hermite–Galerkin spectral method, quadratic collision operator, supersingularity, Burnett polynomials

**AMS subject classifications.** 65M70, 82D10, 65N35

**DOI.** 10.1137/18M1230268

## 1. Introduction.

The Fokker–Planck–Landau (FPL) equation is a common kinetic model in plasma physics, accelerator physics, and astrophysics. It describes binary collisions between charged particles with long-range Coulomb interaction and is represented by a nonlinear partial integro-differential equation.

As a classical result, the FPL operator is the limit of the Boltzmann operator for a sequence of scattering cross sections which converge in a convenient sense to a delta function at zero scattering angle [8]. The original derivation of the equation based on this idea is due to Landau [22], and then several works have been devoted to this problem, such as [2, 12, 30]. Recently, Villani [34] has obtained a rigorous proof of this asymptotic problem in the space homogeneous scenario. For the mathematical properties of the FPL equation, such as the existence of the solutions, we refer the reader to Villani [33] and the reference therein.

The numerical solution of the nonlinear kinetic equations, such as the FPL equation, also represents a real challenge for numerical analysts. This is essentially due to the nonlinearity as well as the high dimension of variables, which is seven for the full problem. Moreover, the complex three-dimensional integro-differential stiff advection-diffusion operator in velocity space is also remarkably difficult to deal with due to the high singularity. Besides, this integration has to be handled carefully since it is

*Submitted to the journal's Computational Methods in Science and Engineering section December 3, 2018; accepted for publication (in revised form) March 16, 2020; published electronically June 8, 2020.

https://doi.org/10.1137/18M1230268

**Funding:** The work of the first author was supported by the National Natural Science Foundation of China through grant 91630310 and by the Science Challenge Project through grant TZ2016002. The work of the second author was supported by the National Natural Science Foundation of China through grants 11501042 and U1930402, by the Chinese Postdoctoral Science Foundation through grant 2018M631233, and by the Science Challenge Project through grant TZ2016002.

†CAPT, LMAM, and School of Mathematical Sciences, Peking University, Beijing 100871, People's Republic of China (rli@math.pku.edu.cn).

‡Beijing Computational Science Research Center, Beijing 100193, People's Republic of China; College of Engineering, Peking University, Beijing 100871, People's Republic of China (ylwang@csrc.ac.cn, wangyanli@pku.edu.cn).

§School of Mathematical Sciences, Peking University, Beijing 100871, China, (roywangyx@pku.edu.cn).

closely related to the macroscopic properties, for example, the preservation of total mass, momentum, and energy under the collision term. Several numerical approaches have been proposed to solve the FPL equation. Generally speaking, there are two kinds of methods in the literature: stochastic methods and deterministic methods. The DSMC method as a stochastic method, which is widely used in the simulation of the Boltzmann equation [4], has been adopted to solve the FPL equation. A detailed discussion about the stochastic method is beyond the scope of this paper, and we refer the reader to [15, 5] for a much more complete treatment. For the deterministic methods, due to the complex form of the FPL operator, several numerical approaches are devoted instead to the simpler diffusive Fokker–Planck (FP) model [17, 38], the space homogeneous situations in the isotropic case [6], or cylindrically symmetric problems [27]. Moreover, Villani [35] has brought up a linear collision model for the Maxwell molecules. The construction of conservative and entropy schemes for the space homogeneous case has been proposed in [13, 7], where the main physical properties are all satisfied. However, the direct implementations of such schemes are all quite expensive. Several fast approximating algorithms to reduce the complexity of these methods, based on multipole expansion [23] or multigrid techniques [6], have been proposed. A fast spectral method based on Fourier spectral approximation of the collision operator is introduced in [26], and it is then also utilized to solve an inhomogeneous FPL equation [37, 16]. For the numerical stiffness of the FP collision operator, the implicit time scheme is also studied [24, 32]. There is a certain kind of asymptotic-preserving method that seeks to accelerate the solution of the FPL equation by the so-called penalization techniques [21].

As another kind of spectral method, the Hermite spectral method is utilized to solve the FPL equation in our work. The Hermite method, where basis functions with weighted orthogonality in $\mathbb{R}^3$ are employed, dates back to Grad's work [19], where it was used to solve the Boltzmann equation and has been known as the moment method ever since. Besides, the expansion with respect to Burnett polynomials is proposed in [9, 18] to find the coefficients of the expansion of the collision term in the Hermite basis. Using the Hermite expansion, it is still a tough job to evaluate the exact coefficients in the expansion of the collision operator since the computational cost for the singular quadratic form is hardly bearable and novel models need to be introduced. The computational time of one evaluation of the collision operator is proportional to the cube of the number of degrees of freedom, while in the Fourier spectral method, the time complexity for a direct Galerkin discretization is only the square of the number of modes. With the fast algorithms, it can be reduced in to $\mathcal{O}(N \log(N))$, where $N$ is the number of modes. In a recent work [36], the explicit expressions of all the coefficients in the Hermite spectral method for the quadratic Boltzmann collision operator are presented, and the new collision model which can preserve the physical properties and reduce computational cost at the same time is brought up using these coefficients. It is much harder to evaluate these coefficients for the quadratic FPL collision operator compared to the Boltzmann equation because of the high singularity and the operator of partial derivative. In [28], the coefficients for the Coulombian case were evaluated numerically, and the explicit form was listed for the first few moments.

Inspired by these works, we, in this paper are devoted to the numerical method for the quadratic collision term of the FPL equation, which may be very singular. Following the approach in [36], we approximate the collision model as the combination of a simple linear term and a quadratic term. The idea is to take only a portion of the truncated series expansion to be treated "quadratically," and the remaining

part is approximated by the linearized FPL operator [25] or the even simpler linear collision operator for the Maxwellian molecules brought up by Villani [35]. This may greatly reduce the computational cost, and we can still capture the evolution of physical variables accurately. The linear terms can be handled easily, while the difficulty imposed by the singularity in the quadratic collision model remains. We reveal that by making use of Burnett polynomials, the singular part of the integral in the collision operator can be handled smoothly. For the typical case that the repulsive force between molecules is proportional to a negative power of their distance, our method can handle problems for index of the power of distance up to $-5$, in comparison to the index fixed as $-3$ in [28]. After dealing with the remaining part in the quadratic term without singularity, the Hermite–Galerkin spectral method is then adopted. We derive the explicit formulae for all the coefficients in the Hermite expansion of the collision operator, and these formulae can all be evaluated exactly offline for immediate applications. Thus, eventually the quadratic term is able to be evaluated efficiently.

The rest of this paper is organized as follows. In section 2, we briefly review the FPL equation and the Hermite expansion of the distribution function. In section 3, we first give an explicit expression of the series expansion of the quadratic collision operator and then introduce precisely how to deal with the singularity by Burnett polynomials. The construction of the approximated collision model is presented in section 4. Some numerical experiments verifying the effectiveness of our methods are carried out in section 5. The concluding remarks and detailed derivation of the expansions are given in section 6 and Appendix A, respectively.

**2. FPL equation and Hermite expansion.** We will first give a brief review of the FPL equation and then introduce the Hermite spectral method for the expansion of the distribution function.

**2.1. FPL equation.** The FPL equation is a prevalent kinetic model in plasma physics, describing the state of the particles in terms of a distribution function $f(t, \boldsymbol{x}, \boldsymbol{v})$, where $t$ is the time coordinate, $\boldsymbol{x}$ represents the spatial coordinates, and $\boldsymbol{v}$ stands for the velocity of particles. The governing equation of $f$ is

$$\frac{\partial f}{\partial t} + \nabla_{\boldsymbol{x}} \cdot (\boldsymbol{v} f) = \mathcal{Q}[f], \qquad t \in \mathbb{R}^+, \quad \boldsymbol{x} \in \mathbb{R}^3, \quad \boldsymbol{v} \in \mathbb{R}^3, \tag{2.1}$$

where $\mathcal{Q}[f]$ is the collision operator with a quadratic form

$$\mathcal{Q}[f](t, \boldsymbol{x}, \boldsymbol{v}) = \nabla_{\boldsymbol{v}} \cdot \int_{\mathbb{R}^3} A(\boldsymbol{v} - \boldsymbol{v}_*)(f(\boldsymbol{v}_*)\nabla_{\boldsymbol{v}} f(\boldsymbol{v}) - f(\boldsymbol{v})\nabla_{\boldsymbol{v}_*} f(\boldsymbol{v}_*))\, \mathrm{d}\boldsymbol{v}_*, \tag{2.2}$$

where $A$ depends on the interaction between particles and is a $3 \times 3$ negative and symmetric matrix in the form [26] of

$$A(\boldsymbol{v}) = \Psi(|\boldsymbol{v}|)\Pi(\boldsymbol{v}), \tag{2.3}$$

with $\Psi$ being a nonnegative radial function and $\Pi(\boldsymbol{v})$ the orthogonal projection upon the space orthogonal to $\boldsymbol{v}$ as $\Pi_{ij}(\boldsymbol{v}) = \delta_{ij} - \frac{v_i v_j}{|\boldsymbol{v}|^2}$.

We are primarily concerned with the inverse power law (IPL) model, for which the force between two molecules is always repulsive and proportional to a power of their distance. In this case, the function $\Psi(\boldsymbol{v})$ has the form

$$\Psi(\boldsymbol{v}) := \Lambda |\boldsymbol{v}|^{\gamma+2}, \tag{2.4}$$

where $\Lambda > 0$ is a constant and $\gamma$ is the index of the power of distance. This equation is obtained as a limit of the Boltzmann equation, when all the collisions become grazing [14]. As in the case of the Boltzmann equation, different $\gamma$ lead to different models. The case $\gamma > 0$ corresponds to the "hard potential" case, whereas for $\gamma < 0$, it corresponds to the case of "soft potential." In the critical case $\gamma = 0$, the gas molecules are referred to as "Maxwell molecules." Another case of interest is when $\gamma = -3$ of the Coulombian case, a very important model for applications in plasma.

We shall focus on the numerical approximation of $\mathcal{Q}[f]$, especially when $\gamma$ is very small. Our model of approximating the collision operator is best illustrated in the spatially homogeneous FPL equation case, namely,

$$\frac{\partial f}{\partial t} = \mathcal{Q}[f], \qquad t \in \mathbb{R}^+, \quad \boldsymbol{v} \in \mathbb{R}^3. \tag{2.5}$$

As a classical result in kinetic equations, the steady-state solution of this equation takes the form of the Maxwellian:

$$\mathcal{M}_{\rho,\boldsymbol{u},\theta}(\boldsymbol{v}) := \frac{\rho}{(2\pi\theta)^{3/2}} \exp\left(-\frac{|\boldsymbol{v}-\boldsymbol{u}|^2}{2\theta}\right), \tag{2.6}$$

where the density $\rho$, velocity $\boldsymbol{u}$, and temperature $\theta$ are defined as follows:

$$\rho = \int_{\mathbb{R}^3} f(t,\boldsymbol{v})\,\mathrm{d}\boldsymbol{v}, \quad \boldsymbol{u} = \frac{1}{\rho}\int_{\mathbb{R}^3} \boldsymbol{v} f(t,\boldsymbol{v})\,\mathrm{d}\boldsymbol{v}, \quad \theta = \frac{1}{3\rho}\int_{\mathbb{R}^3} |\boldsymbol{v}-\boldsymbol{u}|^2 f(t,\boldsymbol{v})\,\mathrm{d}\boldsymbol{v}. \tag{2.7}$$

Moreover, the physical variables, such as the heat flux $q_i$, and the stress tensor $\sigma_{ij}$, are also of interest. They are defined as

$$q_i = \frac{1}{2}\int_{\mathbb{R}^3} |\boldsymbol{v}-\boldsymbol{u}|^2 (v_i - u_i) f\,\mathrm{d}\boldsymbol{v}, \qquad i = 1,2,3,$$
$$\sigma_{ij} = \int_{\mathbb{R}^3} \left((v_i-u_i)(v_j-u_j) - \frac{1}{3}\delta_{ij}|\boldsymbol{v}-\boldsymbol{u}|^2\right) f\,\mathrm{d}\boldsymbol{v}, \quad i,j = 1,2,3.$$

Similar to the Boltzmann equation, the collision operator preserves in time the macroscopic quantities mass, momentum, and energy. Therefore, those are invariant quantities under evolution, and (2.7) holds for any $t$. Thus, we can obtain

$$\rho = 1, \quad \boldsymbol{u} = 0, \quad \theta = 1 \tag{2.8}$$

by selecting a proper frame of reference and applying appropriate nondimensionalization. Now the Maxwellian (2.6) is simply reduced to

$$\mathcal{M}(\boldsymbol{v}) := \frac{1}{(2\pi)^{3/2}} \exp\left(-\frac{|\boldsymbol{v}|^2}{2}\right). \tag{2.9}$$

The heat flux and stress tensor are reduced into

$$q_i = \frac{1}{2}\int_{\mathbb{R}^3} |\boldsymbol{v}|^2 v_i f\,\mathrm{d}\boldsymbol{v}, \qquad \sigma_{ij} = \int_{\mathbb{R}^3} \left(v_i v_j - \frac{1}{3}\delta_{ij}|\boldsymbol{v}|^2\right) f\,\mathrm{d}\boldsymbol{v}, \quad i,j = 1,2,3.$$

The normalization (2.8) shall always be assumed in the following context.

In the literature, the complicated form of the collision operator $\mathcal{Q}[f]$ is handled by introducing approximations of less complexity. For instance, for the Maxwell molecules with $\Lambda = 1$, if the distribution function $f$ is radially symmetric, which is a

property to be preserved under time evolution, the collision operator can be rewritten as

$$\mathcal{Q}^{\text{linear}}[f] = (D-1)\nabla_{\boldsymbol{v}} \cdot (\nabla f + f\boldsymbol{v}), \tag{2.10}$$

as proposed by Villani [35]. Here $D$ is the dimension of the velocity space, and we always set $D = 3$ in the context. In this case, the FPL equation is reduced into the linear FP equation, which can be used to describe the relation of Brownian molecules in a gas.

A more complicated model based on the linearization around equilibrium is also relevant in the literature:

$$\mathcal{L}_{\mathcal{M}}[f] = Q(\mathcal{M}, f) + Q(f, \mathcal{M}). \tag{2.11}$$

We would like to remark that the idea of linearization is similar to the linearized Boltzmann operator. Such a reduced model is of higher accuracy for non-Maxwellian molecules. Properties of the linearized operator and estimations of its error compared with the original FPL model can be found in the literature.

Due to the complex form of the FPL operator, several numerical approaches are devoted to the simpler diffusive FP model or to the reduced collision models [29, 3]. Hence, it is of high necessity to develop efficient numerical methods for the original FPL equation with the quadratic collision operator.

**2.2. Series expansion of distribution function.** Our numerical discretization shall be based on the series expansion in the weighted $L^2$ space of the distribution function $\mathcal{F} = L^2(\mathbb{R}^3; \mathcal{M}^{-1}\,\mathrm{d}\boldsymbol{v})$:

$$f(t, \boldsymbol{v}) = \sum_{|\alpha|=0}^{+\infty} f_\alpha(t) H^\alpha(\boldsymbol{v}) \mathcal{M}(\boldsymbol{v}), \tag{2.12}$$

where $\mathcal{M}(\boldsymbol{v})$ is the Maxwellian $\alpha = (\alpha_1, \alpha_2, \alpha_3)^T$ is a three-dimensional multi-index, and $|\alpha| = \alpha_1 + \alpha_2 + \alpha_3$. In (2.12), $H^\alpha(\boldsymbol{v})$ are the Hermite polynomials defined as follows.

Definition 1 (Hermite polynomials). *For $\alpha_i \in \mathbb{N}, i = 1, 2, 3$, the Hermite polynomial $H^\alpha(\boldsymbol{v})$ is defined as*

$$H^\alpha(\boldsymbol{v}) = \frac{(-1)^n}{\mathcal{M}(\boldsymbol{v})} \frac{\partial^{|\alpha|}}{\partial v_1^{\alpha_1} \partial v_2^{\alpha_2} \partial v_3^{\alpha_3}} \mathcal{M}(\boldsymbol{v}), \tag{2.13}$$

*where $\mathcal{M}(\boldsymbol{v})$ is given in* (2.9).

The expansion (2.2) was introduced to solve Boltzmann equations [19], where such an expansion was invoked to deploy moment methods. We can derive moments based on the coefficients $f_\alpha$ from the orthogonality of Hermite polynomials

$$\int_{\mathbb{R}^3} H^\alpha(\boldsymbol{v}) H^\beta(\boldsymbol{v}) \mathcal{M}(\boldsymbol{v})\,\mathrm{d}\boldsymbol{v} = \delta_{\alpha,\beta}\alpha!, \tag{2.14}$$

where $\delta_{\alpha,\beta}$ is defined as $\delta_{\alpha,\beta} = \prod_{i=1}^3 \delta_{\alpha_i,\beta_i}$ and $\alpha! = \prod_{i=1}^3 \alpha_i!$. For example, by the orthogonality aforementioned, we can insert the expansion (2.12) into the definition of $\rho$ in (2.7) to get $f_{\mathbf{0}} = \rho$, where $\mathbf{0} = (0, 0, 0)$. In our case, the normalization (2.8)

gives us $f_{\mathbf{0}} = 1$. In a similar manner, we can see from the other two equations in (2.7) and (2.8) that

$$f_{e_i} = 0, \quad i = 1, 2, 3, \qquad \sum_{i=1}^{3} f_{2e_i} = 0, \tag{2.15}$$

where $e_i$ is a three-dimensional index whose $i$th entry equals 1 and other entries equal zero. The heat flux and stress tensor are related to the coefficients by

$$q_j = 2f_{3e_j} + \sum_{k=1}^{3} f_{e_j+2e_k}, \qquad \sigma_{ij} = (1+\delta_{ij}) f_{e_i+e_j}, \qquad i, j = 1, 2, 3.$$

**3. Approximation of quadratic collision term.** In order to investigate the evolution of the coefficients $f_\alpha$ in the expansion (2.12), we shall expand the collision term under the same function space. The expansion of the collision operator of the linear type is rather straightforward. As an example, the explicit form of expansion of (2.10) in the three-dimensional case is

$$\mathcal{Q}^{\text{linear}}[f] = \sum_{|\alpha|=0}^{+\infty} Q_\alpha^{\text{linear}} H^\alpha(\boldsymbol{v}) \mathcal{M}(\boldsymbol{v}), \qquad Q_\alpha^{\text{linear}} = -(D-1)|\alpha| f_\alpha, \tag{3.1}$$

which can be proved using Fourier transformation [35] and comes as a consequence of the property that Hermite polynomials diagonalize the linear FP operator. It is also intrinsically implied by the fact that FP equation can be used in the context of stochastic processes, while Hermite polynomials play a crucial role in Brownian motion, but we shall not take the stochastic perspective here.

We shall first discuss the series expansion of the quadratic collision term $\mathcal{Q}[f]$ defined in (2.2) and then combine the quadratic result with the linear-type collision operators to construct collision models with better accuracy and less computational complexity.

**3.1. Series expansions of quadratic collision terms.** Suppose the binary collision term $\mathcal{Q}[f]$ is expanded into the following form:

$$\mathcal{Q}[f](\boldsymbol{v}) = \sum_{|\alpha|=0}^{+\infty} Q_\alpha H^\alpha(\boldsymbol{v}) \mathcal{M}(\boldsymbol{v}). \tag{3.2}$$

Due to the orthogonality of Hermite polynomials, we get

$$Q_\alpha = \frac{1}{\alpha!} \int H^\alpha(\boldsymbol{v}) \mathcal{Q}[f](\boldsymbol{v}) \, \mathrm{d}\boldsymbol{v} = \sum_{|\lambda|=0}^{+\infty} \sum_{|\kappa|=0}^{+\infty} A_\alpha^{\lambda,\kappa} f_\lambda f_\kappa, \tag{3.3}$$

where the last equality can be derived by inserting (2.12) into (2.2), and

$$A_\alpha^{\lambda,\kappa} = \frac{1}{\alpha!} \int_{\mathbb{R}^3} H^\alpha(\boldsymbol{v}) \nabla_{\boldsymbol{v}} \cdot \int_{\mathbb{R}^3} A(\boldsymbol{v} - \boldsymbol{v}_*) \Big( H^\lambda(\boldsymbol{v}_*) \mathcal{M}(\boldsymbol{v}_*) \nabla_{\boldsymbol{v}} \left( H^\kappa(\boldsymbol{v}) \mathcal{M}(\boldsymbol{v}) \right) - H^\lambda(\boldsymbol{v}) \mathcal{M}(\boldsymbol{v}) \nabla_{\boldsymbol{v}_*} \left( H^\kappa(\boldsymbol{v}_*) \mathcal{M}(\boldsymbol{v}_*) \right) \Big) \, \mathrm{d}\boldsymbol{v}_* \, \mathrm{d}\boldsymbol{v}. \tag{3.4}$$

The above formula is of an extremely complex form, with the evaluation of every single coefficient requiring a six-dimensional integration as well as differential operations.

Granted this can be computed by numerical quadrature, the computational cost would be unbearble for getting all these coefficients. Recently, in [28], a strategy to simplify the above integral is introduced for the Coulombian case $\gamma = -3$, and the explicit values are given with small indices. In order to deal with this integral, we give the explicit expressions of all the coefficients $A_\alpha^{\lambda,\kappa}$ and enlarge the applicable region of these expressions to $\gamma > -5$ for the quadratic collision kernel, which incorporates the domain of definition for $\gamma$ in the IPL model. The main results are summarized in the following theorem.

THEOREM 1. *The expansion coefficients of the collision operator $\mathcal{Q}[f](\boldsymbol{v})$ defined in* (3.3) *have the following form:*

$$A_\alpha^{\lambda,\kappa} = 2^{(\gamma+3-|\alpha|)/2} \sum_{s,t=1}^{3} \sum_{|p|=0}^{|\alpha|-1} \frac{\Lambda}{q^{[s]}!} \left( a_{p,r^{[t]}}^{\kappa+e_t,\lambda} - a_{p,r^{[t]}}^{\lambda,\kappa+e_t} \right) B_{r^{[t]}}^{q^{[s]}}(\gamma, s, t), \tag{3.5}$$

*where $p = (p_1, p_2, p_3)^T$ is a three-dimensional multi-index and*

$$q^{[s]} = \alpha - e_s - p, \quad r^{[t]} = \lambda + \kappa + e_t - p, \quad a_{p,q}^{\lambda,\kappa} = \prod_{i=1}^{3} a_{p_i q_i}^{\lambda_i \kappa_i}, \qquad s,t = 1,2,3, \tag{3.6}$$

*the sum is taken for the indices in the range if and only if each subindex is nonnegative.*

*The coefficients $a_{pq}^{\lambda\kappa}$ and $B_p^q(\gamma, s, t)$ are defined by*

$$a_{pq}^{\lambda\kappa} = 2^{-(p+q)/2} \lambda! \kappa! \sum_{s=\max(0,p-\kappa)}^{\min(p,\lambda)} \frac{(-1)^{q-\lambda+s}}{s!(\lambda-s)!(p-s)!(q-\lambda+s)!} \tag{3.7}$$

*and*

$$B_p^q(\gamma, s, t) := -G_{st}(\gamma, p, q) + \delta_{st} \sum_{r=1}^{3} G_{rr}(\gamma, p, q), \tag{3.8}$$

*where*

$$G_{st}(\gamma, p, q) = \int_{\boldsymbol{g} \in \mathbb{R}^3} |\boldsymbol{g}|^\gamma g_s g_t H^p(\boldsymbol{g}) H^q(\boldsymbol{g}) \mathcal{M}(\boldsymbol{g}) \, \mathrm{d}\boldsymbol{g}, \qquad s,t = 1,2,3. \tag{3.9}$$

The proof of Theorem 1 can be found in Appendix A.1. Hence, we only have to compute (3.9). When $\gamma > -3$, it can be computed directly by the recursive formula of the Hermite polynomials following the method in [36]. However, for the Coulombian case $\gamma = -3$, the recursive formula cannot be adopted directly due to the singularity induced by the small value of $\gamma$. In [28], the Coulombian case $\gamma = -3$ is evaluated by adopting the special form of the quadratic collision term there. In the next section, we will introduce a new method to deal with the supersingularity for a large region of $\gamma$.

**3.2. Derivation of exact coefficients in supersingular integral.** In this section, we will introduce a different method to calculate these coefficients exactly, and the applicable area of $\gamma$ is enlarged as well. In order to deal with the singularity, Burnett polynomials, products of Sonine polynomials, and solid spherical harmonics [20] are utilized here. Burnett polynomials are introduced in [9] to approximate the distribution function of the Boltzmann equation and was adopted in [10, 18] for the

quadratic collision operator. To be concrete, the normalized form of the Burnett polynomials is

$$B_{\hat{\alpha}}(\boldsymbol{v}) = \sqrt{\frac{2^{1-\hat{\alpha}_1}\pi^{3/2}\hat{\alpha}_3!}{\Gamma(\hat{\alpha}_3+\hat{\alpha}_1+3/2)}} L_{\hat{\alpha}_3}^{(\hat{\alpha}_1+1/2)}\left(\frac{|\boldsymbol{v}|^2}{2}\right)|\boldsymbol{v}|^{\hat{\alpha}_1} Y_{\hat{\alpha}_1}^{\hat{\alpha}_2}\left(\frac{\boldsymbol{v}}{|\boldsymbol{v}|}\right),$$

where the index $\hat{\alpha}$ is defined as

$$\hat{\alpha} = (\hat{\alpha}_1, \hat{\alpha}_2, \hat{\alpha}_3)^T, \quad \hat{\alpha}_1, \hat{\alpha}_3 \in \mathbb{N}, \quad \hat{\alpha}_2 = -\hat{\alpha}_1, \ldots, \hat{\alpha}_1.$$

Here $L_n^{(\beta)}(x)$ is the Laguerre polynomials

$$L_n^{(\beta)}(x) = \frac{x^{-\beta}\exp(x)}{n!}\frac{\mathrm{d}^n}{\mathrm{d}x^n}\left[x^{n+\beta}\exp(-x)\right],$$

and $Y_l^m(\boldsymbol{n})$ is spherical harmonics

$$Y_l^m(\boldsymbol{n}) = \sqrt{\frac{2l+1}{4\pi}\frac{(l-m)!}{(l+m)!}} P_l^m(\cos\theta)\exp(\mathrm{i}m\phi), \quad \boldsymbol{n} = (\sin\theta\cos\phi, \sin\theta\sin\phi, \cos\theta)^T$$

with $P_l^m$ the associate Legendre polynomial

$$P_l^m(x) = \frac{(-1)^m}{2^l l!}(1-x^2)^{m/2}\frac{\mathrm{d}^{l+m}}{\mathrm{d}x^{l+m}}\left[(x^2-1)^l\right].$$

By the orthogonality of Laguerre polynomials and spherical harmonics, one can find that

$$\int_{\mathbb{R}^3} \overline{B_{\hat{\alpha}}(\boldsymbol{v})} B_{\hat{\beta}}(\boldsymbol{v})\mathcal{M}(\boldsymbol{v})\,\mathrm{d}\boldsymbol{v} = \delta_{\hat{\alpha},\hat{\beta}}. \tag{3.10}$$

In order to reduce complexity, the symmetry of $G_{st}(\gamma,p,q)$, which is stated in Lemma 2, is utilized first to reduce the cost of computation and storage.

LEMMA 2. *For the expressions $G_{st}(\gamma,p,q)$, it holds that*

$$G_{st}(\gamma,p,q) = G_{ts}(\gamma,p,q), \qquad s,t = 1,2,3, \tag{3.11}$$

*and*

$$\begin{aligned} &G_{11}(\gamma,p,q) = G_{22}(\gamma,\Pi_2^1 p,\Pi_2^1 q) = G_{33}(\gamma,\Pi_3^1 p,\Pi_3^1 q),\\ &G_{12}(\gamma,p,q) = G_{13}(\gamma,\Pi_3^2 p,\Pi_3^2 q) = G_{23}(\gamma,\Pi_3^1 p,\Pi_3^1 q). \end{aligned} \tag{3.12}$$

*Here $\Pi_i^j p$ is a permutation operator which exchanges the $i$th and $j$th entries of $p$.*

Based on Lemma 2, we only have to compute two cases $G_{33}(\gamma,p,q)$ and $G_{13}(\gamma,p,q)$. In order to handle the singularity in $G_{st}(\gamma,p,q)$, Hermite polynomials in (3.9) are expressed by a linear combination of the Burnett polynomials, precisely,

$$H^\alpha(\boldsymbol{v}) = \sum_{|\hat{\alpha}|_B=|\alpha|} C_{\hat{\alpha}}^\alpha B_{\hat{\alpha}}(\boldsymbol{v}), \qquad C_{\hat{\alpha}}^\alpha = \int_{\mathbb{R}^3} B_{\hat{\alpha}}(\boldsymbol{v})H^\alpha(\boldsymbol{v})\mathcal{M}(\boldsymbol{v})\,\mathrm{d}\boldsymbol{v}, \tag{3.13}$$

where $|\hat{\alpha}|_B = \hat{\alpha}_1 + 2\hat{\alpha}_3$. Since both Hermite and Burnett polynomials are orthogonal polynomials associated with the same weight function, the coefficients $C_{\hat{\alpha}}^\alpha$ defined in (3.13) are nonzero only when the degrees of $H^\alpha$ and $B_{\hat{\alpha}}$ are equal, precisely, $|\hat{\alpha}|_B = |\alpha|$. The detailed algorithm to compute the coefficient $C_{\hat{\alpha}}^\alpha$ can be found in [10], and we also explain that briefly in Appendix A.3. With the help of the Burnett polynomials, we can finally get the exact value of $G_{st}(\gamma,p,q)$.

PROPOSITION 3. *When $\gamma > -5$, $G_{st}(\gamma, p, q)$ defined in* (3.9) *can be simplified as*

$$G_{st}(\gamma,p,q) = 2^{(\gamma+2)/2} \sum_{|\hat{p}|_B=|p|} \sum_{|\hat{q}|_B=|q|} C_{\hat{p}}^{p} C_{\hat{q}}^{q} D_{\hat{p}_3,\hat{q}_3}^{\hat{p}_1\hat{q}_1} K\left(\frac{\gamma+\hat{p}_1+\hat{q}_1+3}{2}, \hat{p}_1+\frac{1}{2}, \hat{q}_1+\frac{1}{2}, \hat{p}_3, \hat{q}_3\right) F_{st}(\hat{p}_1,\hat{p}_2,\hat{q}_1,\hat{q}_2), \tag{3.14}$$

*where*

$$F_{st}(\hat{p}_1,\hat{p}_2,\hat{q}_1,\hat{q}_2) = \int_{\mathbb{S}^2} n_s n_t Y_{\hat{p}_1}^{\hat{p}_2}(\boldsymbol{n}) Y_{\hat{q}_1}^{\hat{q}_2}(\boldsymbol{n})\,\mathrm{d}\boldsymbol{n}, \qquad s,t=1,2,3, \tag{3.15}$$

*where $n_s$ and $n_t$ are the $s$th and $t$th entries of the unit vector $\boldsymbol{n}$ in spherical coordinates $\boldsymbol{n} = (\sin\theta\cos\phi, \sin\theta\sin\phi, \cos\theta)^T$. The parameters in* (3.14) *are defined as*

$$D_{n_1 n_2}^{l_1 l_2} = \sqrt{\frac{n_1! n_2!}{\Gamma(n_1+l_1+3/2)\Gamma(n_2+l_2+3/2)}}$$

*and*

$$K(\mu,\alpha,\kappa,m,n) = (-1)^{m+n}\Gamma(\mu+1) \sum_{i=0}^{\min(m,n)} \binom{\mu-\alpha}{m-i}\binom{\mu-\kappa}{n-i}\binom{i+\mu}{i}. \tag{3.16}$$

*Proof.* Substituting (3.13) into (3.9) and adopting the formula introduced in [31, eq. (10)],

$$\int_0^{+\infty} L_m^{(\alpha)}(s) L_n^{(\kappa)}(s) s^{\mu} \exp(-s)\,\mathrm{d}s = (-1)^{m+n}\Gamma(\mu+1) \sum_{i=0}^{\min(m,n)} \binom{\mu-\alpha}{m-i}\binom{\mu-\kappa}{n-i}\binom{i+\mu}{i}, \tag{3.17}$$

we have thus validated this proposition. ∎

Finally, as stated previously in Lemma 2, we only need to compute $G_{33}(\gamma,p,q)$ and $G_{13}(\gamma,p,q)$. Therefore, only these two corresponding cases of (3.15) are discussed in the following theorem, and the proof is presented in Appendix A.2.

THEOREM 4. *Define $\eta_{lm}^{\mu}$ as*

$$\eta_{lm}^{\mu} = \sqrt{\frac{[l+(2\delta_{1,\mu}-1)m+\delta_{1,\mu}][l-(2\delta_{-1,\mu}-1)m+\delta_{-1,\mu}]}{2^{|\mu|}(2l-1)(2l+1)}}. \tag{3.18}$$

*Then the coefficients $F_{13}(l_1,m_1,l_2,m_2)$ and $F_{33}(l_1,m_1,l_2,m_2)$ have the following explicit form:*

(3.19)

$$F_{13}(l_1,m_1,l_2,m_2) = \frac{(-1)^{m_2+1}}{\sqrt{2}} \sum_{k,j,l=0,1} (-1)^{l+j} \eta^{0}_{\delta_{0k}+(-1)^k l_2, m_2} \eta^{(-1)^l}_{(-1)^j l_1+\delta_{0j}, m_1} \delta^{m_1+(-1)^l, -m_2}_{l_1+\delta_{1k}-\delta_{1j}, l_2-\delta_{1k}+\delta_{1j}},$$

$$F_{33}(l_1,m_1,l_2,m_2) = (-1)^{m_2} \sum_{k,j=0,1} \eta^{0}_{\delta_{0k}+(-1)^k l_2, m_2} \eta^{0}_{(-1)^j l_1+\delta_{0j}, m_1} \delta^{m_1, -m_2}_{l_1+\delta_{1k}-\delta_{1j}, l_2-\delta_{1k}+\delta_{1j}}.$$

The above analysis shows that for the FPL collision operator, the coefficients $A_\alpha^{\lambda,\kappa}$ can be calculated exactly for $\gamma > -5$, which makes it much easier to build the high-order scheme to numerically solve the FPL equation. Moreover, this algorithm for the coefficients here is readily applicable for offline numerical evaluation, the effectiveness of which is corroborated by our numerical examples.

**4. Construction of novel collision model.** We already obtained a complete algorithm to calculate the coefficients $A_\alpha^{\lambda,\kappa}$, which can be utilized either to obtain the expansion of the quadratic collision term or to construct new collision models. We will now discuss both topics.

**4.1. Discretization of homogeneous FPL equation.** We will reformulate the homogeneous FPL equation by the Galerkin spectral method in terms of the expansion of the distribution function (2.12). For any positive integer $M$, we define as the functional space of numerical solution

$$\mathcal{F}_M = \mathrm{span}\{H^\alpha(v)M(v)|\alpha \in I_M\} \subset \mathcal{F} = L^2(\mathbb{R}^3; \mathcal{M}^{-1}dv), \tag{4.1}$$

where $I_M = \{(\alpha_1, \alpha_2, \alpha_3)|0 \leqslant |\alpha| \leqslant M, \alpha_i \in \mathbb{N}, i = 1, 2, 3\}$. Then the semidiscrete function $f_M(t, \cdot) \in \mathcal{F}_M$ satisfies

$$\int_{\mathbb{R}^3} \frac{\partial f_M}{\partial t}\varphi\mathcal{M}^{-1}\,\mathrm{d}\boldsymbol{v} = \int_{\mathbb{R}^3} \mathcal{Q}(f_M, f_M)\varphi\mathcal{M}^{-1}\,\mathrm{d}\boldsymbol{v} \qquad \forall\varphi \in \mathcal{F}_M. \tag{4.2}$$

Suppose

$$f_M(t, \boldsymbol{v}) = \sum_{\alpha\in I_M} f_\alpha(t)H^\alpha(\boldsymbol{v})\mathcal{M}(\boldsymbol{v}) \in \mathcal{F}_M. \tag{4.3}$$

The equations (3.2) and (3.3) imply that the variational form (4.2) is equivalent to the ODE system below:

$$\frac{\mathrm{d}f_\alpha}{\mathrm{d}t} = \sum_{\lambda\in I_M}\sum_{\kappa\in I_M} A_\alpha^{\lambda,\kappa} f_\lambda f_\kappa, \qquad \alpha \in I_M. \tag{4.4}$$

We thus obtain the formulation of the ODE system in its full form (4.4), with the help of the exact coefficients $A_\alpha^{\lambda,\kappa}$ for all $\alpha, \lambda, \kappa \in I_M$. With $M$ fixed, these coefficients need to be computed only once and then can be used repeatedly for multiple numerical examples.

**4.2. Approximation to general collision model.** In practical computation, the storage cost of computing the coefficients $A_\alpha^{\lambda,\kappa}$ is formidably expensive, as the number of coefficients increases significantly with $M$ increasing. Moreover, the computational cost $O(M^9)$ is an issue especially when solving the spatially nonhomogeneous problems.

To overcome this difficulty, the method in [36] is utilized to reduce the computational cost, precisely, that the coefficients $A_\alpha^{\lambda,\kappa}$ for a small number $M_0$ are computed and stored when the computational cost for solving (4.4) is acceptable. As for $\alpha \notin I_{M_0}$, we apply the linear model (2.10) brought up by Villani and compute as

$$\frac{\mathrm{d}f_\alpha}{\mathrm{d}t} = -(D-1)|\alpha|f_\alpha, \qquad \alpha \notin I_{M_0}. \tag{4.5}$$

Another alternative for the linear model would be the one with a guarantee of theoretical approximation (2.11). We can compute the expansion of the linearized

operator and its associated ODE system with the help of the coefficients already computed:

$$\mathcal{L}_M[f] = \sum_{\alpha\in I_M,\kappa\in I_M} \left(A_\alpha^{0,\kappa} + A_\alpha^{\kappa,0}\right) f_\kappa H^\alpha(\boldsymbol{v})\mathcal{M}(\boldsymbol{v}), \tag{4.6}$$

$$\frac{\mathrm{d}f_\alpha}{\mathrm{d}t} = \sum_{\kappa\in I_M} A_\alpha^{0,\kappa} f_\kappa + A_\alpha^{\kappa,0} f_\kappa, \qquad \alpha \notin I_{M_0}. \tag{4.7}$$

Combining (4.4) and (4.5) or (4.7), we obtain a novel collision operator

$$\mathcal{Q}^{M_0}[f] = P_{M_0}\mathcal{Q}[P_{M_0}f] + (I - P_{M_0})\mathcal{Q}^{\mathrm{linear}}[f] \qquad \forall f \in \mathcal{F}, \tag{4.8}$$

where $P_{M_0}$ is the orthogonal projection from $\mathcal{F}$ onto $\mathcal{F}_{M_0}$. After applying the spectral method to this collision operator in the functional space $\mathcal{F}_M$, where $M$ is chosen to be larger than $M_0$, the final ODE system for the new model is

$$\frac{\mathrm{d}f_\alpha}{\mathrm{d}t} = \mathcal{Q}_\alpha^{M,M_0}, \tag{4.9}$$

where

$$\mathcal{Q}_\alpha^{M,M_0} = \begin{cases} \displaystyle\sum_{\lambda\in I_{M_0}}\sum_{\kappa\in I_{M_0}} A_\alpha^{\lambda,\kappa} f_\lambda f_\kappa, & \alpha \in I_{M_0}, \\ -(D-1)|\alpha| f_\alpha, & \alpha \in I_M \setminus I_{M_0}. \end{cases} \tag{4.10}$$

Or, alternatively, if we replace $\mathcal{Q}^{\mathrm{linear}}$ with $\mathcal{L}_M$ in (4.8), we obtain an alternative to (4.10)

$$\mathcal{Q}_\alpha^{M,M_0} = \begin{cases} \displaystyle\sum_{\lambda\in I_{M_0}}\sum_{\kappa\in I_{M_0}} A_\alpha^{\lambda,\kappa} f_\lambda f_\kappa, & \alpha \in I_{M_0}, \\ \displaystyle\sum_{\kappa\in I_M} A_\alpha^{0,\kappa} f_\kappa + A_\alpha^{\kappa,0} f_\kappa, & \alpha \in I_M \setminus I_{M_0}. \end{cases} \tag{4.11}$$

We have obtained a series of new collision models (4.8). It can be expected that such combination could reduce the time cost significantly due to the simple form of the linear FP collision operator in the Hermite basis while at the same time managing to maintain a high level of accuracy since the evolution function already captures the most crucial information in coefficients of lower order and performs a satisfactory approximation in the other coefficients. This will be observed in the numerical examples.

**5. Numerical examples.** In this section, we shall present several results in our numerical computation. In all of the numerical experiments, we shall adopt the newly proposed collision operator (4.8) and solve the equation

$$\frac{\partial f}{\partial t} = \mathcal{Q}^{M_0}[f]$$

numerically for some positive integer $M_0$. Such an equation is solved by the Galerkin spectral method for solution defined in the functional space $\mathcal{F}_M$, with $M$ chosen to be greater than $M_0$. Namely, we solve the system of ODE (4.10). As for the discretization in time, we use the fourth-order Runge–Kutta method in the examples, and the time step is chosen as $\Delta t = 0.01$. In the examples, we shall set $\Lambda = 1$.

Finally, we would like to mention that the derivation of the expansion coefficients in the Hermite basis are exact in each case by mathematical derivation instead of numerical integration in order to achieve high accuracy.

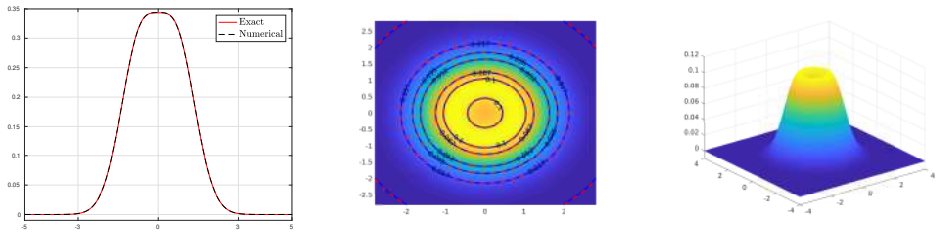


(a) Initial MDF $g(0, v_1)$ (b) Contours of $h(0, v_1, v_2)$ (c) Initial MDF $h(0, v_1, v_2)$

FIG. 1. (a) *Initial marginal distribution functions* $g(0, v_1)$. *The red solid line corresponds to the exact solution, and the blue dashed line corresponds to the numerical approximation.* (b) *Initial marginal distribution functions* $h(0, v_1, v_2)$. *The blue solid lines correspond to the exact solution, and the red dashed lines correspond to the numerical approximation.* (c) *The numerical approximation only.*

**5.1. BKW solution.** For the Maxwell gas $\gamma = 0$, the original FPL equation admits an exact solution with the following expression:

$$f(t, \boldsymbol{v}) = (2\pi\tau(t))^{-3/2} \exp\left(-\frac{|\boldsymbol{v}|^2}{2\tau(t)}\right)\left[1 + \frac{1-\tau(t)}{\tau(t)}\left(\frac{|\boldsymbol{v}|^2}{2\tau(t)} - \frac{3}{2}\right)\right],$$

where $\tau(t) = 1 - 0.4\exp(-4t)$. As a good approximation of the initial distribution function, we use $M = 15$ (816 degrees of freedom) in our simulation. For visualization purposes, we define the marginal distribution functions (MDFs)

$$g(t, v_1) = \int_{\mathbb{R}^2} f(t, \boldsymbol{v})\, \mathrm{d}v_2\, \mathrm{d}v_3, \qquad h(t, v_1, v_2) = \int_{\mathbb{R}} f(t, \boldsymbol{v})\, \mathrm{d}v_3.$$

The initial MDFs are plotted in Figure 1, in which the lines for exact functions and their numerical approximation are hardly distinguishable.

Numerical results for $t = 0.01$, $0.02$, and $0.06$ are given in Figures 2 and 3, respectively, for the marginal distribution function $g(t, v_1)$ and $h(t, v_1, v_2)$. Here we set $M_0$ as $M_0 = 5$ and 15. For $M_0 = 5$, the numerical solution provides a reasonable approximation but still with noticeable deviations, while for $M_0 = 15$, the two solutions match perfectly in all cases. To study the computational time, we run the simulation for $M_0 = 3, \ldots, 15$ until $t = 1$ in a single CPU core with model Intel Core i7-6700. The average computational time for a single collision operator with different $M_0$ is in Table 1, and the relation between the total computational time, the value of $M_0$, and the total number of freedom $N_{M_0}$ corresponding to $M_0$ is plotted in Figure 4. Here $N_{M_0}$ is the total number of freedom when the expansion order is $M_0$ in (4.1) as

$$N_{M_0} = \frac{(M_0+1)(M_0+2)(M_0+3)}{6}. \tag{5.1}$$

It can be seen that the computational time is roughly proportional to the cube of the number of degrees of freedom. Since the computational time also includes the time for processing the coefficients of basis functions with degree between $M_0$ and $M$, the computational time is greatly affected by this linear part when $M_0$ is small. Though the time complexity is only linear, the number of such coefficients is quite large, and they have a significant contribution to the total computational time.

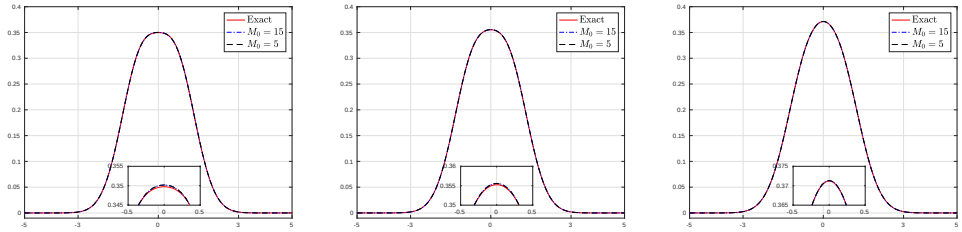


(a) $t = 0.02$ (b) $t = 0.02$ (c) $t = 0.02$

FIG. 2. *Marginal distribution functions $g(t, v_1)$ for $M_0 = 5$ and $M_0 = 15$ at $t = 0.01$, 0.02, and 0.06. The red solid lines correspond to the exact solution, and the blue dot dashed and black dashed lines correspond to the numerical solutions with $M_0 = 15$ and $M_0 = 5$, respectively.*

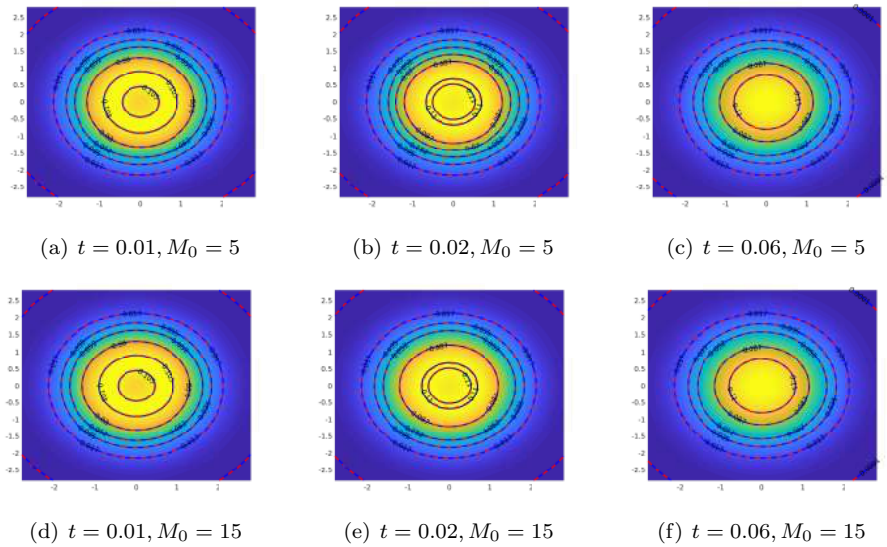

(a) $t = 0.01, M_0 = 5$ (b) $t = 0.02, M_0 = 5$ (c) $t = 0.06, M_0 = 5$

(d) $t = 0.01, M_0 = 15$ (e) $t = 0.02, M_0 = 15$ (f) $t = 0.06, M_0 = 15$

FIG. 3. *Marginal distribution functions $h(t, v_1, v_2)$ for $M_0 = 5$ and $M_0 = 15$ at $t = 0.01$, 0.02, and 0.06. The red dashed lines correspond to the exact solution, and the blue solid lines at different columns correspond to the numerical solutions $M_0 = 5$ and $M_0 = 15$.*

TABLE 1
*Average computational time for a single collision operator for different values of $M_0$.*

| $M_0$ | 3 | 4 | 5 | 6 | 7 | 8 | 9 |
|---|---|---|---|---|---|---|---|
| Time (ms) | 0.0006 | 0.0007 | 0.0008 | 0.0018 | 0.0051 | 0.0119 | 0.0240 |
| $M_0$ | 10 | 11 | 12 | 13 | 14 | 15 | |
| Time (ms) | 0.0472 | 0.0911 | 0.1655 | 0.2944 | 0.4914 | 0.7941 | |

Now we consider the time evolution of the expansion coefficients. By expanding the exact solution into Hermite series, we get the exact solution for the coefficients:

$$f_\alpha(t) = \begin{cases} [-0.2\exp(-4t)]^{\frac{|\alpha|}{2}} \dfrac{1 - |\alpha|/2}{(\alpha_1/2)!(\alpha_2/2)!(\alpha_3/2)!} & \text{if } \alpha_1, \alpha_2, \alpha_3 \text{ are even,} \\ 0 & \text{otherwise.} \end{cases} \tag{5.2}$$

From (5.2), we can find that the coefficients $f_\alpha$ are zero for any $t$ if $1 \leqslant |\alpha| \leqslant 3$. Hence,

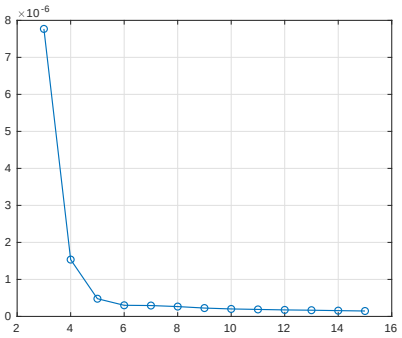


FIG. 4. *The relation between the computational time and the value of $M_0$. The horizontal axis is the value of $M_0$, and the vertical axis is the value of $T_{M_0}/N_{M_0}^3$.*

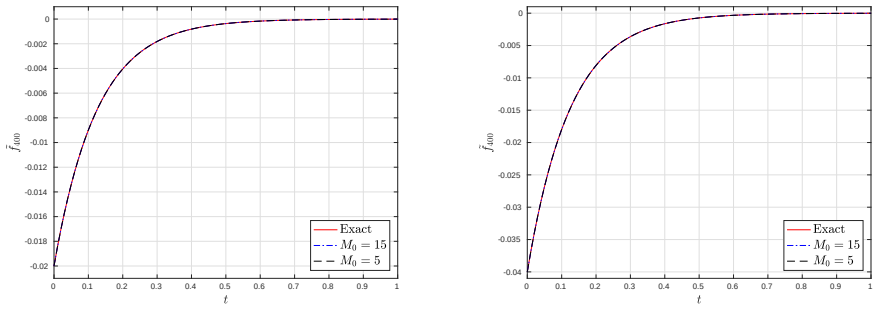


(a) $f_{400}(t)$ (b) $f_{220}(t)$

FIG. 5. *The evolution of the coefficients. The red lines correspond to the reference solution, and the blue dot dashed and black dashed lines correspond to the numerical solutions of $M_0 = 15$ and $M_0 = 5$, respectively.*

we will focus on the coefficients $f_{400}$ and $f_{220}$ here. Figure 5 gives the comparison between the numerical solution and the exact solution for these two coefficients. In both plots, all the three lines coincide perfectly.

**5.2. Bi-Gaussian initial data.** In this example, we perform the numerical test for the bi-Gaussian problem. Here the Coulombian case $\gamma = -3$ is tested. The initial distribution function is

$$f(0,\boldsymbol{v}) = \frac{1}{2\pi^{3/2}}\left[\exp\left(-(v_1+\sqrt{3/2})^2+v_2^2+v_3^2\right)+\exp\left(-(v_1-\sqrt{3/2})^2+v_2^2+v_3^2\right)\right].$$

In this numerical test, we use $M = 20$, which gives a good approximation of the initial distribution function (see Figure 6).

For this example, we consider the three cases $M_0 = 5, 10$, and 15, and the corresponding one-dimensional marginal distribution functions at $t = 0.4$, 1, and 3 are given in Figure 7. In all the results, the numerical results are converging to the reference solution as $M_0 = 15$, and the lines for $M_0 = 10$ and $M_0 = 15$ are very close to each other. To get a clearer picture, similar comparisons of two-dimensional results are also provided in Figure 8.

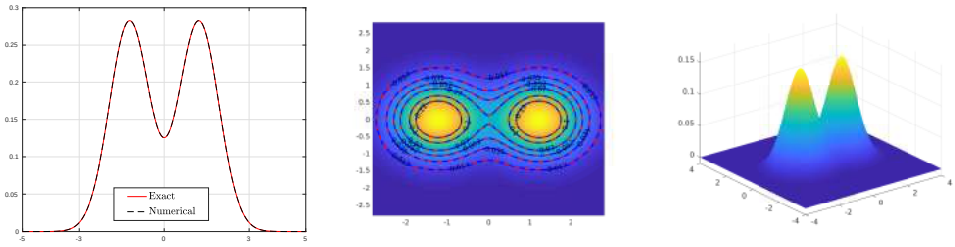


(a) Initial MDF $g(0, v_1)$ (b) Contours of $h(0, v_1, v_2)$ (c) Initial MDF $h(0, v_1, v_2)$

FIG. 6. (a) *Initial marginal distribution functions* $g(0, v_1)$. *The red solid line corresponds to the exact solution, and the blue dashed line corresponds to the numerical approximation.* (b) *Initial marginal distribution functions* $h(0, v_1, v_2)$. *The blue solid lines correspond to the exact solution, and the red dashed lines correspond to the numerical approximation.* (c) *The numerical approximation only.*

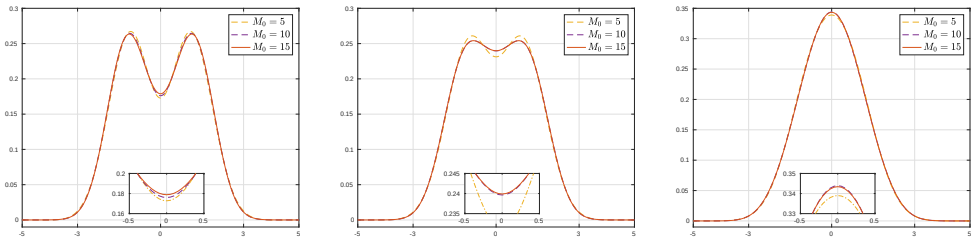


(a) $t = 0.4$ (b) $t = 1$ (c) $t = 3$

FIG. 7. *The Coulombian case* $\gamma = -3$. *Marginal distribution functions at different times.*

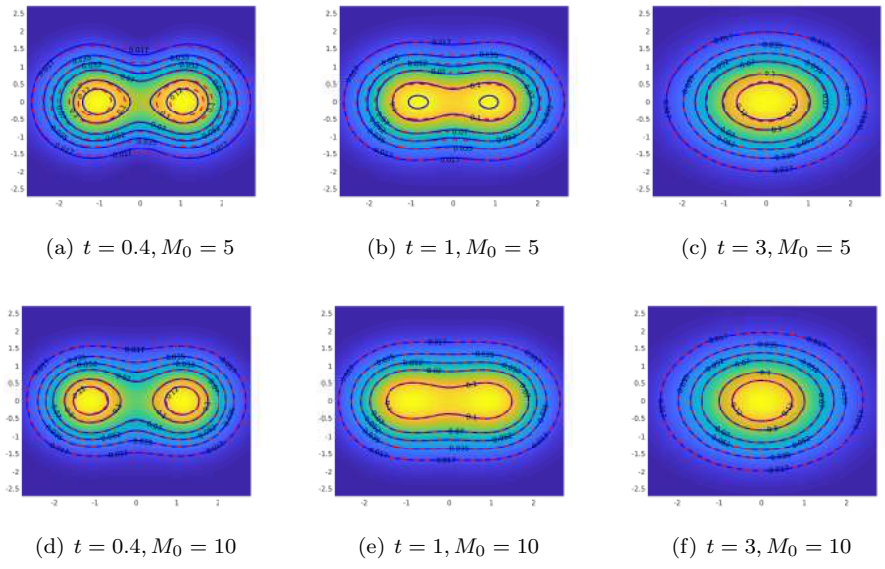

(a) $t = 0.4, M_0 = 5$ (b) $t = 1, M_0 = 5$ (c) $t = 3, M_0 = 5$

(d) $t = 0.4, M_0 = 10$ (e) $t = 1, M_0 = 10$ (f) $t = 3, M_0 = 10$

FIG. 8. *The Coulombian case* $\gamma = -3$. *Comparison of numerical results with the reference solution. The red dashed contours are the reference solution as* $M_0 = 15$. *The blue solid contours at different columns are, respectively, the results for* $M_0 = 5$ *and* $M_0 = 10$.

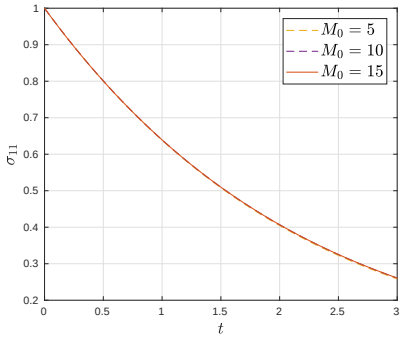


FIG. 9. *The Coulombian case $\gamma = -3$. Evolution of $\sigma_{11}(t)$. Three lines are on top of each other.*

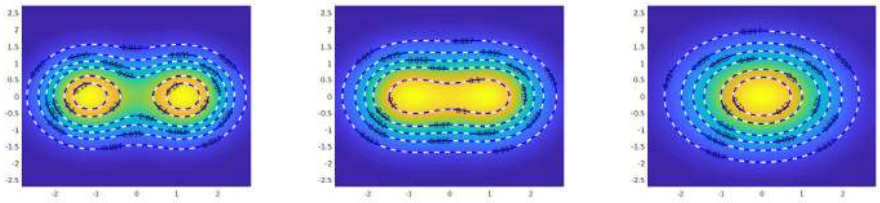

(a) $t = 0.4$ (b) $t = 1$ (c) $t = 3$

FIG. 10. *The Coulombian case $\gamma = -3$. Comparison of numerical solutions obtained by Hermite spectral method and the Fourier spectral method. The white dashed contours are the solutions obtained by the Hermite spectral method with $M_0 = 15$ and $M = 20$. The blue solid contours are the numerical solutions obtained by the Fourier method.*

Now we consider the evolution of the stress tensor and heat flux. In this example, we always have $\sigma_{11} = -2\sigma_{22} = -2\sigma_{33}$ and $q_i = 0, i = 1, 2, 3$. Therefore, we focus only on the evolution of $\sigma_{11}$, which is plotted in Figure 9. It can be seen that even for $M_0 = 5$, the evolution of the stress tensor is almost exact, where the distribution function is not approximated very well. The three lines are all on top of each other.

In order to validate the combined collision model, we compare the results obtained from the Hermite spectral method with that from the Fourier spectral method. Here the number of nodes for the Fourier method is set as $N = 20$, where the degree of freedom is 68921. In the Hermite spectral method, $M_0$, $M$ are chosen as $M_0 = 15$ and $M = 20$, where the degree of freedom is 1771. In Figure 10, we can see that the numerical solutions for the Fourier spectral method and the Hermite method are on top of each other, which shows the reliability of the Hermite method.

In order to test the computational capacity of our new model, the same example with a very small $\gamma$ as $\gamma = -4.9$ is tested. Here we also set $M = 20$ and choose the numerical results with $M_0 = 15$ as the reference solution. Figure 11 shows the marginal distribution $h(t, v_1, v_2)$ at $t = 0.4, 1$, and 3 with $M_0 = 5$ and $M_0 = 10$. It illustrates that when $\gamma$ equals $-4.9$, the numerical solutions are converging to the reference solution as $M_0 = 15$ and that the solution with $M_0 = 10$ is almost the same as the reference solution. The time evolution of $\sigma_{11}$ is plotted in Figure 12, where the three results are also on top of each other, even with $M_0 = 5$. Moreover, from Figures 11 and 12, we can find that the time evolution of the distribution function with $\gamma = -4.9$ is slower than that with $\gamma = -3$, which is also consistent with the form of the FPL collision operator.

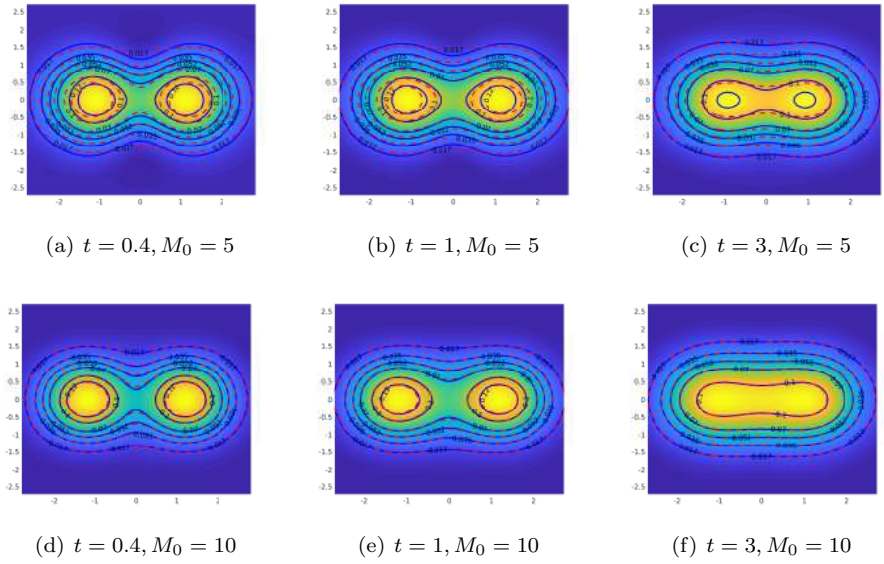

(a) $t = 0.4, M_0 = 5$ (b) $t = 1, M_0 = 5$ (c) $t = 3, M_0 = 5$

(d) $t = 0.4, M_0 = 10$ (e) $t = 1, M_0 = 10$ (f) $t = 3, M_0 = 10$

FIG. 11. *The case $\gamma = -4.9$. Comparison of numerical solutions and the reference solution. The red dashed contours are the reference solutions $M_0 = 15$. The blue solid contours at different columns are, respectively, the numerical solutions $M_0 = 5$ and $M_0 = 10$.*

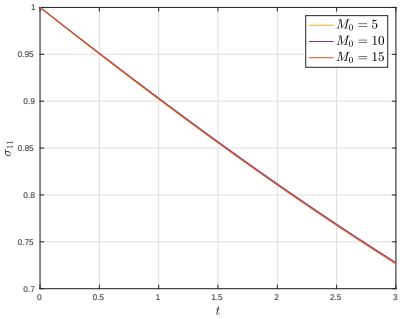


FIG. 12. *The case $\gamma = -4.9$. Evolution of $\sigma_{11}(t)$. Three lines are on top of each other.*

**5.3. Rosenbluth problem.** In this example, the Rosenbluth problem is tested. Also, the Coulombian case $\gamma = -3$ and the case $\gamma = -4.9$ are tested. The initial condition is from [26] as

$$f(0, \boldsymbol{v}) = A \exp(-(B|\boldsymbol{v}| - 1)^2). \tag{5.3}$$

The parameter $A, B$ is standardized to satisfy the condition that the initial density and temperature all equal 1, precisely,

$$A = \frac{(b/3)^{3/2}}{a^{5/2}}, \qquad B = \frac{(b/3)^{1/2}}{a^{1/2}}, \tag{5.4}$$

where $a = \pi(3\sqrt{\pi}(\mathrm{erf}(1) + 1 + 2/e)$ and $b = \pi(9.5\sqrt{\pi}(\mathrm{erf}(1) + 1) + 7/e)$. Here $e$ is the Euler number, and $\mathrm{erf(x)} = \frac{1}{\sqrt{\pi}} \int_0^{\mathrm{x}} \mathrm{e}^{-\mathrm{t}^2}\,\mathrm{dt}$ is the error function.

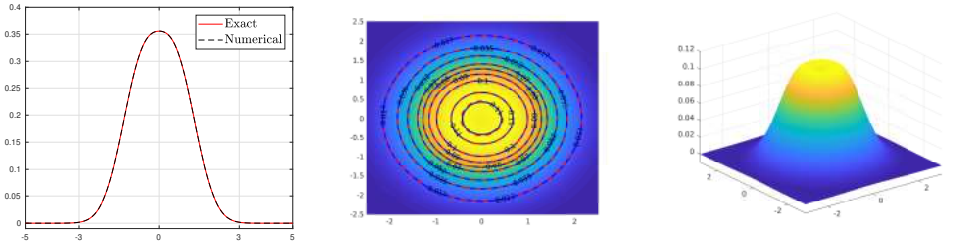


(a) Initial MDF $g(0, v_1)$ (b) Contours of $h(0, v_1, v_2)$ (c) Initial MDF $h(0, v_1, v_2)$

FIG. 13. (a) *Initial marginal distribution function* $g(0, v_1)$. *The red solid line corresponds to the exact solution, and the blue dashed line corresponds to the numerical approximation.* (b) *Initial marginal distribution functions* $h(0, v_1, v_2)$. *The blue solid lines correspond to the exact solution, and the red dashed lines correspond to the numerical approximation.* (c) *The numerical approximation only.*

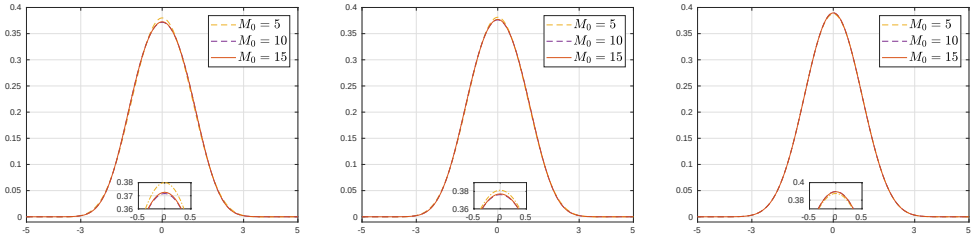


(a) $t = 0.4$ (b) $t = 0.6$ (c) $t = 2$

FIG. 14. *The Coulombian case* $\gamma = -3$. *Marginal distribution functions at different times.*

In order to approximate the initial distribution function well, in this numerical test, we set $M = 40$. The initial MDFs are plotted in Figure 13, which illustrates the perfect numerical approximation to the exact distribution function.

For this example, the three cases $M_0 = 5, 10$, and 15 are tested also. The numerical solution with $M_0 = 15$ is treated as the reference solution. The corresponding one- and two-dimensional marginal distribution functions for the Coulombian $\gamma = -3$ are shown in Figures 14 and 15, where the numerical solutions are converging to the reference solution and that with $M_0 = 10$ is almost the same as the reference solution.

Similarly, the comparisons of the numerical solutions between the Hermite spectral method and the Fourier spectral method are shown in Figure 16. Here the number of nodes for the Fourier method is set as $N = 20$, and $M_0$, $M$ are chosen as $M_0 = 15$ and $M = 20$ in the Hermite spectral method, respectively. We can see that for the Rosenbluth problem, the numerical solutions of the Hermite spectral method also match well with those of the Fourier spectral method, which also validates the Hermite spectral method proposed in this paper.

Moreover, our new model can also approximate the $\gamma = -4.9$ case well. The two-dimensional marginal distribution functions for $\gamma = -4.9$ are presented in Figure 17. The numerical solution with $M_0 = 15$ is also chosen as the reference solution. Similar to the example in section 5.2, the time evolution of the distribution function with $\gamma = -4.9$ is also slower than that with $\gamma = -3$. Furthermore, though there are distinct differences between the numerical solution $M_0 = 5$ and $M_0 = 15$, the numerical solutions are converging to the reference solutions $M_0 = 15$.

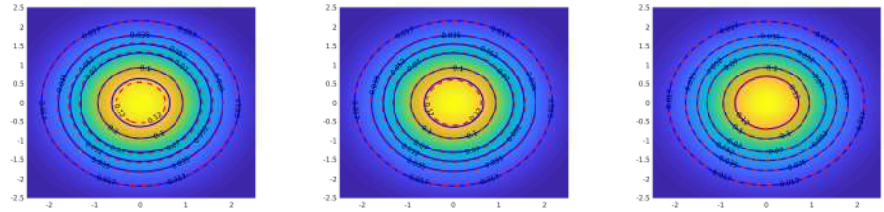

(a) $t = 0.4, M_0 = 5$ (b) $t = 0.6, M_0 = 5$ (c) $t = 2, M_0 = 5$

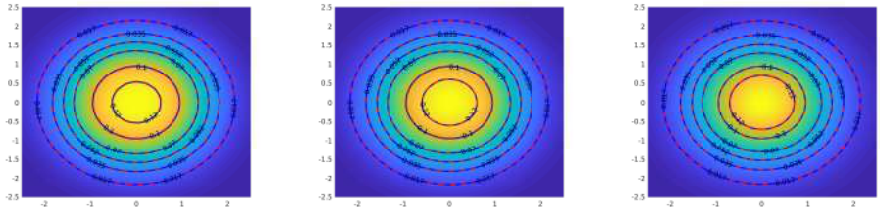

(d) $t = 0.4, M_0 = 10$ (e) $t = 0.6, M_0 = 10$ (f) $t = 2, M_0 = 10$

FIG. 15. *The Coulombian case $\gamma = -3$. Comparison of numerical solutions and the reference solution $M_0 = 15$. The red dashed contours are the reference solution. The blue solid contours in different columns are, respectively, the numerical solutions $M_0 = 5$ and $M_0 = 10$.*

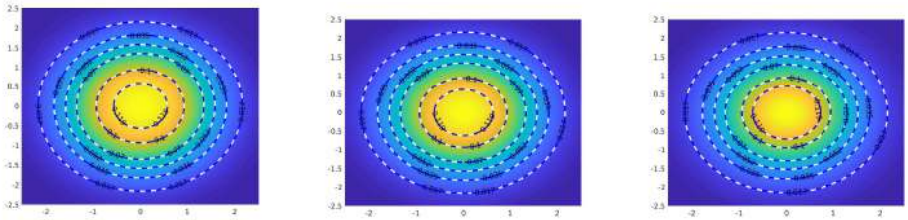

(a) $t = 0.4$ (b) $t = 1$ (c) $t = 2$

FIG. 16. *The Coulombian case $\gamma = -3$. Comparison of numerical solutions obtained by the Hermite spectral method and the Fourier spectral method. The white dashed contours are the solutions obtained by the Hermite spectral method with $M_0 = 15$ and $M = 20$. The blue solid contours are the numerical solutions obtained by the Fourier method.*

**6. Conclusion.** In this paper, we focus on applying the Hermite spectral method to develop an efficient and accurate way of approximating and numerically solving the FPL equation. Basic properties of Hermite polynomials are utilized to obtain a simplified expression of the coefficients which renders the numerical method feasible. Burnett polynomials are introduced to deal with the supersingular integral in the computation. This method could cover more practical cases up to $\gamma > -5$.

A novel collision model is built with a combination of a quadratic collision model and a linear approximation model with reduced complexity. The original model is of complexity $O(N^3)$ for $N$ as the number of moments. Good candidates for such a linear model consist of the linear FP collision model and the linearized FPL operator. The former one is an approximation based on the case of Maxwellian molecules and has complexity $O(N)$, while the latter is more involved, based on linearization around

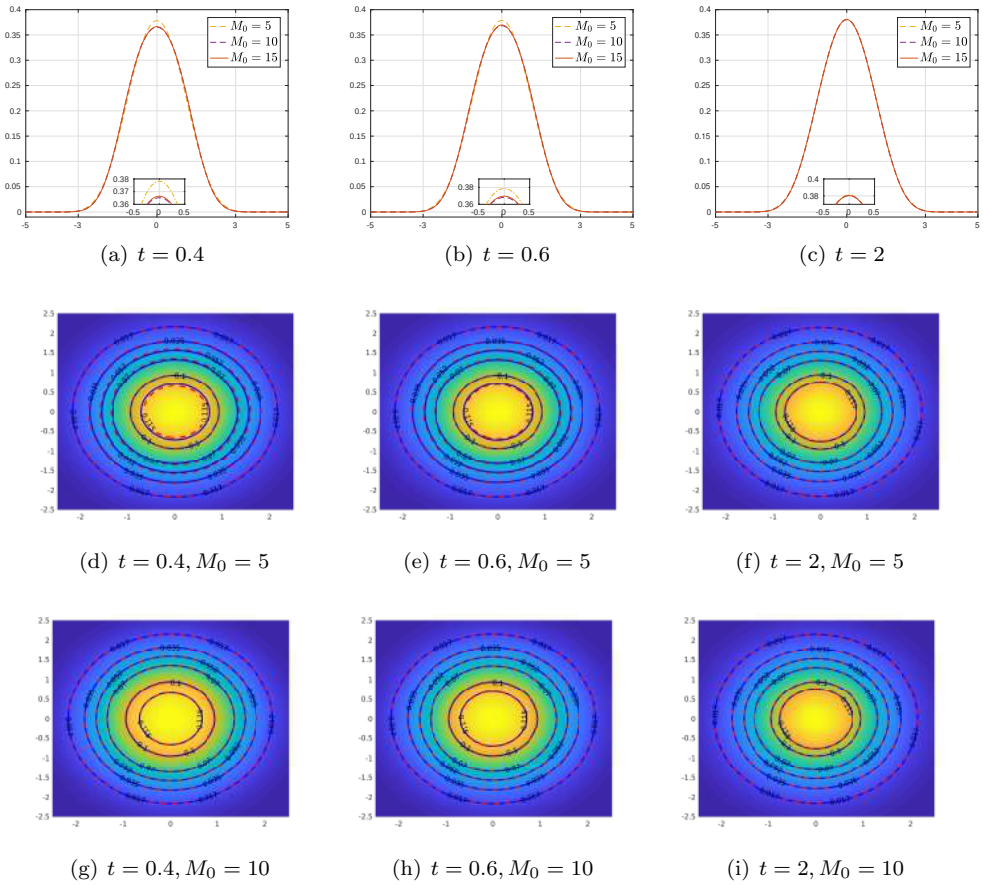


(a) $t = 0.4$ (b) $t = 0.6$ (c) $t = 2$

(d) $t = 0.4, M_0 = 5$ (e) $t = 0.6, M_0 = 5$ (f) $t = 2, M_0 = 5$

(g) $t = 0.4, M_0 = 10$ (h) $t = 0.6, M_0 = 10$ (i) $t = 2, M_0 = 10$

FIG. 17. *The Coulombian case $\gamma = -4.9$. Marginal distribution functions at different times. The first row is the marginal distribution $g(t, v_1)$, and the latter two rows are the marginal distribution functions $h(t, v_1, v_2)$ with different $M_0$. The red dashed contours are the reference solutions $M_0 = 15$. The blue solid contours at different rows are, respectively, the numerical solutions when $M_0 = 5$ and $M_0 = 10$.*

equilibrium with desired theoretic accuracy and complexity $O(N^2)$. The numerical experiments validate the efficiency of this new model. With the model introduced, the numerical solutions are of a high accuracy and at an affordable computational cost. This method should be further validated in the numerical tests for the full FPL equation with spatial variables, which will be one of the future works.

## Appendix A.

**A.1. Proof of Theorem 1.** We shall present of proof of Theorem 1 here. In order to prove Theorem 1, we first introduce the lemma below.

LEMMA 5. *Let $\boldsymbol{v} = \boldsymbol{h} + \boldsymbol{g}/2$ and $\boldsymbol{w} = \boldsymbol{h} - \boldsymbol{g}/2$. It holds that*

$$H^{\alpha}(\boldsymbol{v})H^{\kappa}(\boldsymbol{w}) = \sum_{\alpha'+\kappa'=\alpha+\kappa} a^{\alpha\kappa}_{\alpha'\kappa'} H^{\alpha'}(\sqrt{2}\boldsymbol{h}) H^{\kappa'}\left(\frac{\boldsymbol{g}}{\sqrt{2}}\right), \tag{A.1}$$

*where the coefficients $a^{\alpha\kappa}_{\alpha'\kappa'}$ are defined in* (3.7).

COROLLARY 6. *Let* $\boldsymbol{v} = \boldsymbol{h} + \boldsymbol{g}/2$. *We have*

$$H^{\alpha}(\boldsymbol{v}) = \sum_{\kappa+\lambda=\alpha} \frac{2^{-|\alpha|/2}\alpha!}{\kappa!\lambda!} H^{\kappa}\left(\sqrt{2}\boldsymbol{h}\right) H^{\lambda}\left(\frac{\boldsymbol{g}}{\sqrt{2}}\right).$$

The proof of Lemma 5 can be found in [36]. Next we will prove Theorem 1.

*Proof.* Using an integration by parts and the recursion formula of Hermite polynomials

$$\frac{\partial}{\partial v_s}\Big(\mathcal{M}(\boldsymbol{v})H^{\alpha}(\boldsymbol{v})\Big) = (-1)\mathcal{M}(\boldsymbol{v})H^{\alpha+e_s}(\boldsymbol{v}), \qquad s = 1, 2, 3, \tag{A.2}$$

the coefficients $A_{\alpha}^{\lambda,\kappa}$ (3.4) can be simplified as

$$\begin{aligned} A_{\alpha}^{\lambda,\kappa} = \sum_{s,t=1}^{3} \frac{\Lambda}{(\alpha-e_s)!} \int_{\mathbb{R}^3\times\mathbb{R}^3} |\boldsymbol{v}-\boldsymbol{v}^*|^{\gamma} G_{st}(\boldsymbol{v}-\boldsymbol{v}^*) \\ H^{\alpha-e_s}(\boldsymbol{v}^*)\mathcal{M}(\boldsymbol{v})\mathcal{M}(\boldsymbol{v}^*)\left(H^{\lambda}(\boldsymbol{v}^*)H^{\kappa+e_t}(\boldsymbol{v}) - H^{\lambda}(\boldsymbol{v})H^{\kappa+e_t}(\boldsymbol{v}^*)\right) \mathrm{d}\boldsymbol{v}\,\mathrm{d}\boldsymbol{v}^*, \end{aligned} \tag{A.3}$$

where $G_{st}(\boldsymbol{v}) = -v_s v_t + \delta_{st}|\boldsymbol{v}|^2$. Further simplification of (A.3) follows the method in [36], where the velocity of the mass center is defined as $\boldsymbol{h} = (\boldsymbol{v}+\boldsymbol{v}^*)/2$ and the relative velocity is defined as $\boldsymbol{g} = \boldsymbol{v} - \boldsymbol{v}^*$. Hence, it holds that

$$\boldsymbol{v} = \boldsymbol{h} + \frac{1}{2}\boldsymbol{g}, \quad \boldsymbol{v}^* = \boldsymbol{h} - \frac{1}{2}\boldsymbol{g}, \quad |\boldsymbol{v}|^2 + |\boldsymbol{v}^*|^2 = \frac{1}{2}|\boldsymbol{g}|^2 + 2|\boldsymbol{h}|^2, \qquad \mathrm{d}\boldsymbol{v}\,\mathrm{d}\boldsymbol{v}^* = \mathrm{d}\boldsymbol{g}\,\mathrm{d}\boldsymbol{h}. \tag{A.4}$$

Combining Lemma 5, (A.3), and (A.4), the integral in $A_{\alpha}^{\lambda,\kappa}$ can be rewritten with respect to $\boldsymbol{g}$ and $\boldsymbol{h}$:

$$\begin{aligned} A_{\alpha}^{\lambda,\kappa} = 2^{(\gamma/2+3-|\alpha|)/2} \sum_{s,t=1}^{3} \sum_{p+q=k-e_s} \sum_{r+\beta=\lambda+\kappa} \int_{\mathbb{R}^3\times\mathbb{R}^3} |\boldsymbol{g}|^{\gamma} \frac{\Lambda}{p!q!} G_{st}(\boldsymbol{g}) H^{q}(\boldsymbol{g})\mathcal{M}(\boldsymbol{g})\mathcal{M}(\boldsymbol{h}) \\ \left(a_{(\beta+e_t)r}^{(\kappa+e_t)\lambda} H^{r}(\boldsymbol{g})H^{\beta+e_t}(\boldsymbol{h})H^{p}(\boldsymbol{h}) - a_{r(\beta+e_t)}^{\lambda(\kappa+e_t)} H^{\beta+e_t}(\boldsymbol{g})H^{r}(\boldsymbol{h})H^{p}(\boldsymbol{h})\right) \mathrm{d}\boldsymbol{g}\,\mathrm{d}\boldsymbol{h}. \end{aligned} \tag{A.5}$$

Using the orthogonality of Hermite polynomials, we can finally prove Theorem 1. ∎

**A.2. Proof of Theorem 4.** In order to prove Theorem 4, we will introduce the lemma below.

LEMMA 7. *For three spherical harmonics* $Y_l^m$, $Y_{l_1}^{m_1}$, *and* $Y_{l_2}^{m_2}$, *if* $m \neq m_1 + m_2$ *or* $l \notin [|l_1 - l_2|, l_1 + l_2]$, *then*

$$\int_{\mathbb{S}^2} Y_{l_1}^{m_1}(\boldsymbol{n}) Y_{l_2}^{m_2}(\boldsymbol{n}) \overline{Y_l^m(\boldsymbol{n})}\,\mathrm{d}\boldsymbol{n} = 0. \tag{A.6}$$

*Especially, we have*

$$Y_l^m(\boldsymbol{n})Y_1^{\mu}(\boldsymbol{n}) = \sqrt{\frac{3}{4\pi}}\left(\eta_{l+1,m}^{\mu} Y_{l+1}^{m+\mu}(\boldsymbol{n}) + (-1)^{\mu}\eta_{-l,m}^{\mu} Y_{l-1}^{m+\mu}(\boldsymbol{n})\right), \qquad \mu = -1, 0, 1, \tag{A.7}$$

*where* $\eta_{lm}^{\mu}$ *is defined in* (3.18).

The result of this lemma can be found in section 12.9 of [1].

*Proof.* Note that

$$n_1 = \sqrt{\frac{2\pi}{3}}\left(Y_1^1 - Y_1^{-1}\right), \qquad n_2 = -\mathrm{i}\sqrt{\frac{2\pi}{3}}\left(Y_1^1 + Y_1^{-1}\right), \qquad n_3 = 2\sqrt{\frac{\pi}{3}}Y_1^0. \tag{A.8}$$

Based on Lemma 7 and the property of spherical harmonic

$$\overline{Y_l^m(\boldsymbol{n})} = (-1)^m Y_l^{-m}(\boldsymbol{n}),$$

we can derive the results in Theorem 4 with the orthogonality property of spherical harmonics

$$\int_{\mathbb{S}^2} Y_{l_1}^{m_1}(\boldsymbol{n})\overline{Y_{l_2}^{m_2}(\boldsymbol{n})}\,\mathrm{d}\boldsymbol{n} = \delta_{l_1 l_2}\delta_{m_1 m_2}. \tag{A.9}$$

∎

**A.3. Computation of coefficients $C_{\hat{\boldsymbol{\alpha}}}^{\boldsymbol{\alpha}}$.** In this section, we will briefly introduce the algorithm to calculate $C_{\hat{\alpha}}^{\alpha}$, and the original algorithm is in [10].

Define

$$S_{-1} = \frac{1}{2}(v_1 - \mathrm{i}v_2), \quad S_0 = v_3, \quad S_1 = -\frac{1}{2}(v_1 + \mathrm{i}v_2), \tag{A.10}$$

and the recursive formula of the basis functions [11] is

$$\begin{aligned} S_\mu B_{\hat{\alpha}}(\boldsymbol{v}) = \frac{1}{2^{|\mu|/2}}\Big[&\sqrt{2(\hat{\alpha}_1+\hat{\alpha}_3)+3}\,\eta^\mu_{\hat{\alpha}_1+1,m} B_{\hat{\alpha}+(1,\mu,0)^T}(\boldsymbol{v}) \\ &- \sqrt{2\hat{\alpha}_3}\,\eta^\mu_{\hat{\alpha}_1+1,\hat{\alpha}_2} B_{\hat{\alpha}+(1,\mu,-1)^T}(\boldsymbol{v}) \\ &+ (-1)^\mu\sqrt{2(\hat{\alpha}_3+\hat{\alpha}_1)+1}\,\eta^\mu_{-\hat{\alpha}_1,\hat{\alpha}_2} B_{\hat{\alpha}+(-1,\mu,0)^T}(\boldsymbol{v}) \\ &- (-1)^\mu\sqrt{2(\hat{\alpha}_3+1)}\,\eta^\mu_{-\hat{\alpha}_1,\hat{\alpha}_2} B_{\hat{\alpha}+(-1,\mu,1)^T}(\boldsymbol{v})\Big], \end{aligned} \tag{A.11}$$

where $\eta^\mu_{lm}$ is defined in (3.9), and we set $B_{\hat{\alpha}}(\boldsymbol{v}) = 0$ if $|\hat{\alpha}_2| > \hat{\alpha}_1$ or if either $\hat{\alpha}_1$ or $\hat{\alpha}_3$ is negative. Based on the recursion formula of Hermite polynomials

$$v_s H^\alpha(\boldsymbol{v}) = H^{\alpha+e_s}(\boldsymbol{v}) + k_s H^{\alpha-e_s}(\boldsymbol{v}), \qquad s = 1,2,3, \tag{A.12}$$

we can get the recursive formula to compute $C_{\hat{\alpha}}^{\alpha}$, precisely,

$$\begin{aligned} a^{(-1)}_{\hat{\alpha}+e_2} C^\alpha_{\hat{\alpha}+e_1} + b^{(-1)}_{\hat{\alpha}+e_2} C^\alpha_{\hat{\alpha}-e_1+e_3} &= \frac{1}{2}k_1 C^{\alpha-e_1}_{\hat{\alpha}+e_2} - \frac{\mathrm{i}}{2}k_2 C^{\alpha-e_2}_{\hat{\alpha}+e_2}, \\ a^{(0)}_{\hat{\alpha}} C^\alpha_{\hat{\alpha}+e_1} + b^{(0)}_{\hat{\alpha}} C^\alpha_{\hat{\alpha}-e_1+e_3} &= k_3 C^{\alpha-e_3}_{\hat{\alpha}}, \\ a^{(1)}_{\hat{\alpha}-e_2} C^\alpha_{\hat{\alpha}+e_1} + b^{(1)}_{\hat{\alpha}-e_2} C^\alpha_{\hat{\alpha}-e_1+e_3} &= -\frac{1}{2}k_1 C^{\alpha-e_1}_{\hat{\alpha}-e_2} - \frac{\mathrm{i}}{2}k_2 C^{\alpha-e_2}_{\hat{\alpha}-e_2}, \end{aligned} \tag{A.13}$$

where $|\alpha| = |\hat{\alpha}|_B$ and

$$\begin{aligned} a^{(\mu)}_{\hat{\alpha}} &= \frac{1}{2^{|\mu|/2}}\sqrt{(2(\hat{\alpha}_1+\hat{\alpha}_3)+3)}\,\eta^\mu_{\hat{\alpha}_1+1,\hat{\alpha}_3}, \\ b^{(\mu)}_{\hat{\alpha}} &= \frac{(-1)^{\mu+1}}{2^{|\mu|/2}}\sqrt{2(\hat{\alpha}_3+1)}\,\eta^\mu_{-\hat{\alpha}_1,\hat{\alpha}_3}, \quad \mu = -1,0,1. \end{aligned} \tag{A.14}$$

As is stated in [10], we solve all the coefficients $C_{\hat{\alpha}}^{\alpha}$ by the order of $|\alpha|$, so that the right-hand sides of (A.13) are always known. The initial condition and the boundary conditions are $C_{\mathbf{0}}^{\mathbf{0}} = 1$ and $C_{\hat{\alpha}}^{\alpha} = 0$ if $|\hat{\alpha}_2| > \hat{\alpha}_1$ or if either $\hat{\alpha}_1$ or $\hat{\alpha}_3$ is negative. Moreover, the time complexity for computing all the coefficients $C_{\hat{\alpha}}^{\alpha}$ with $|\hat{\alpha}|_B = |\alpha| \leqslant M$ is $O(M^5)$.

## REFERENCES


[1] G. Arfken and H. Weber, *Mathematical Methods for Physicists*, 6th ed., Academic Press, New York, 2005.

[2] A. Arsen'ev and O. Buryak, *On the connection between a solution of the Boltzmann equation and a solution of the Landau-Fokker-Planck equation*, Math. USSR Sbornik, 69 (1991), p. 465.

[3] Y. Berezin, V. Khudick, and M. Pekker, *Conservative finite-difference schemes for the Fokker-Planck equation not violating the law of an increasing entropy*, J. Comput. Phys., 69 (1987), pp. 163–174.

[4] G. Bird, *Molecular Gas Dynamics and the Direct Simulation of Gas Flows*, Clarendon Press, Oxford, 1994.

[5] A. Bobylev and I. Potapenko, *Monte Carlo methods and their analysis for Coulomb collisions in multicomponent plasma*, J. Comput. Phys., 246 (2013), pp. 123–144.

[6] C. Buet and S. Cordier, *Conservative and entropy decaying numerical scheme for the isotropic Fokker-Planck-Landau equation*, J. Comput. Phys., 145 (1998), pp. 1228–1245.

[7] C. Buet and S. Cordier, *Numerical analysis of conservative and entropy schemes for the Fokker-Planck-Landau equation*, SIAM J. Numer. Anal., 36 (1999), pp. 953–973.

[8] C. Buet, S. Cordier, and F. Filbet, *Comparison of numerical schemes for Fokker-Planck-Landau equation*, ESAIM Proc., 10 (2001), pp. 161–181.

[9] D. Burnett, *The distribution of molecular velocities and the mean motion in a non-uniform gas*, Proc. London Math. Soc., 40 (1936), pp. 382–435.

[10] Z. Cai, Y. Fan, and Y. Wang, *Burnett Spectral Method for the Spatially Homogeneous Boltzmann Equation*, preprint, arXiv:1810.07804, 2018.

[11] Z. Cai and M. Torrilhon, *Numerical simulation of microflows using moment methods with linearized collision operator*, J. Sci. Comput., 74 (2018), pp. 336–374.

[12] P. Degond and B. Lucquin-Desreux, *The Fokker-Planck asymptotics of the Boltzmann collision operator in the Coulomb case*, Math. Models Methods Appl. Sci., 02 (1992), pp. 167–182.

[13] P. Degond and B. Lucquin-Desreux, *An entropy scheme for the Fokker-Planck collision operator of plasma kinetic theory*, Numer. Math., 68 (1994), pp. 239–262.

[14] L. Desvillettes, *On asymptotics of the Boltzmann equation when the collisions become grazing*, Transport. Theor. Stat., 21 (1992), pp. 259–276.

[15] G. Dimarco, R. Caflish, and L. Pareschi, *Direct simulation Monte Carlo schemes for Coulomb interactions in plasma*, Commun. Appl. Ind. Math., 1 (2010), pp. 72–91.

[16] F. Filbet and L. Pareschi, *A numerical method for the accurate solution of the Fokker-Planck-Landau equation in the nonhomogeneous case*, J. Comput. Phys., 179 (2002), pp. 1–26.

[17] J. Fok, B. Guo, and T. Tang, *Combined Hermite spectral-finite difference method for the Fokker-Planck equation*, Math. Comp., 71 (2002), pp. 1497–1528.

[18] I. Gamba and S. Rjasanow, *Galerkin-Petrov approach for the Boltzmann equation*, J. Comput. Phys., 366 (2018), pp. 341–365.

[19] H. Grad, *On the kinetic theory of rarefied gases*, Comm. Pure Appl. Math., 2 (1949), pp. 331–407.

[20] E. Ikenberry and C. Truesdell, *On the pressures and the flux of energy in a gas according to Maxwell's kinetic theory* I, J. Ration. Mech. Anal., 5 (1956), pp. 1–54.

[21] S. Jin and B. Yan, *A class of asymptotic-preserving schemes for the Fokker-Planck-Landau equation*, J. Comput. Phys., 230 (2011), pp. 6420–6437.

[22] L. Landau, *The transport equation in the case of Coulomb interactions*, in Collected Papers of L. Landau, D. Haar, ed., Pergamon, New York, 1965, pp. 163–170, https://doi.org/10.1016/B978-0-08-010586-4.50029-8.

[23] M. Lemou, *Multipole expansions for the Fokker-Planck-Landau operator*, Numer. Math., 78 (1998), pp. 597–618.

[24] M. Lemou and L. Mieussens, *Implicit schemes for the Fokker-Planck-Landau equation*, SIAM J. Sci. Comput., 27 (2005), pp. 809–830.

[25] C. Mouhot, *Explicit coercivity estimates for the linearized Boltzmann and Landau operators*, Comm. Partial Differential Equations, 31 (2006), pp. 1321–1348.

[26] L. Pareschi, G. Russo, and G. Toscani, *Fast spectral methods for the Fokker-Planck-Landau collision operator*, J. Comput. Phys., 165 (2000), pp. 216–236.

[27] M. Pekker and V. Khudik, *Conservative difference scheme for the Fokker-Planck equation*, USSR Comput. Maths. Math. Phys., 24 (1984), pp. 206–210.

[28] D. Pfefferlé, E. Hirvijoki, and M. Lingam, *Exact collisional moments for plasma fluid theories*, Phys. Plasmas, 24 (2017), 042118.
[29] I. Potapenko and C. de Azevedo, *The completely conservative difference schemes for the nonlinear Landau-Fokker-Planck equation*, J. Comput. Appl. Math., 103 (1999), pp. 115–123.
[30] M. Rosenbluth, W. MacDonald, and D. Judd, *Fokker-Planck equation for an inverse-square force*, Phys. Rev., 107 (1957), pp. 1–6.
[31] H. Srivastava, H. Mavromatis, and R. Alassar, *Remarks on some associated Laguerre integral results*, Appl. Math. Lett., 16 (2003), pp. 1131–1136.
[32] W. Taitano, L. Chacón, A. Simakov, and K. Molvig, *A mass, momentum, and energy conserving, fully implicit, scalable algorithm for the multi-dimensional, multi-species Rosenbluth-Fokker-Planck equation*, J. Comput. Phys., 297 (2015), pp. 357–380.
[33] C. Villain, *A review of mathematical topics in collisional kinetic theory*, in Handbook of Mathematical Fluid Dynamics, S. Friedlander and D. Serre, eds., Vol. 1, North Holland, Amsterdam, 2002, pp. 71–305.
[34] C. Villani, *On a new class of weak solutions to the spatially homogeneous Boltzmann and Landau equations*, Arch. Ration. Mech. Anal., 143 (1998), pp. 273–307.
[35] C. Villani, *On the spatially homogeneous Landau equation for Maxwellian molecule*, Math. Models Methods Appl. Sci., 08 (1998), pp. 957–983.
[36] Y. Wang and Z. Cai, *Approximation of the Boltzmann collision operator based on Hermite spectral method*, J. Comput. Phys., 397 (2019), https://doi.org/10.1016/j.jcp.2019.07.014.
[37] C. Zhang and M. Gamba, *Deterministic conservative solver for the inhomogeneous Fokker-Planck-Landau equation coupled with Poisson equation*, AIP Conf. Proc., 1786 (2016), 180008.
[38] D. Zhang, G. Wei, D. Kouri, and D. Hoffman, *Numerical method for the nonlinear Fokker-Planck equation*, Phys. Rev. E, 56 (1997), pp. 1197–1206.